SSRG International Journal of Electrical and Electronics Engineering
ISSN: 2348-8379/ https://doi.org/10.14445/23488379/IJEEE-V12I4P103

Volume 12 Issue 4, 47-62, April 2025

Original Article

Precision Modeling and Comparative Analysis of Photovoltaic Panel Parameters: Integrating Mathematical Approaches and Experimental Validation

K.N. Yogithanjali Saimadhuri[1], M. Janaki[2]

[1,2]*School of Electrical Engineering, VIT, Vellore, Tamilnadu, India.*

[2]*Corresponding Author : janaki.m@vit.ac.in*

Received: 02 February 2025 Revised: 04 March 2025 Accepted: 05 April 2025 Published: 29 April 2025

Abstract - *Photovoltaic systems are becoming more popular as clean and sustainable energy sources. A reliable and flexible PV model must be used at the design stage to accurately estimate the quantity of electricity generated by PV under various operating situations. The performance of PV systems under varying temperature and irradiance levels depends on the accurate extraction of key parameters that define the electrical characteristics of solar cells. This paper focuses on the mathematical modeling of the single diode model and the parameter extraction of five unknown parameters, Ipvref, Ioref, nref, Rsref, and Rpref, at reference and in general conditions. These factors are crucial as they regulate solar cells' current-voltage (I-V) and power-voltage (P-V) properties. This affects the accuracy of performance prediction under varied environmental circumstances. A comparative analysis is performed through numerical and villalva methods. The analysis is carried out with six different solar panels, namely monocrystalline, polycrystalline, PERC, Topcon, HJT, and Kaneka solar PV cells, and the specifications are taken from the manufacturing data sheet. The I-V and P-V characteristics of solar PV cells are investigated at different temperatures and degrees of irradiation. The simulation results are compared with the hardware experimental outputs to verify the retrieved parameters from the two mathematical methodologies. Villalva's method closely matches hardware results compared with the numerical method. In the experiment, a practical test is conducted using the Chroma PV Emulator (62000H-S Series). At 250 W/m2 irradiances, the measured power matches the panel power, with an MPPT test efficiency of 98.78%. To assess the precision of two mathematical approaches, the Root Mean Square Error (RMSE), Mean Bias Error (MBE), and Mean Absolute Error (MAE) are estimated over many operational points.*

Keywords - *Solar PV, Single Diode Model (SDM), Standard Test Condition (STC), Solar PV emulator.*

1. Introduction

Solar energy is one of the most widely available and conveniently accessible energy sources for meeting the world's energy needs. Solar energy has grown in popularity in recent years due to various advantages such as global availability, low maintenance, and ease of installation compared to other renewable energy sources. However, it is impossible to capture the entire amount of energy due to the intermittent nature of sunlight. Many challenges arise while harnessing solar energy due to geographical location, atmospheric conditions, weather uncertainty, temperature variations, etc. The usage of Photovoltaic (PV) technology is critical to reducing greenhouse gas emissions and combating climate change. According to the [1], improvements in PV efficiency have driven acceptance worldwide, positioning solar PV as a crucial component in the shift to a sustainable energy system. [2] emphasizes how India's solar Photovoltaic (PV) business is experiencing tremendous expansion and holds great promise due to technology improvements and legislation that support the sector. It highlights how crucial PV is to economically and sustainably supplying India's electricity needs. [3] highlights the noteworthy developments in solar Photovoltaic (PV) materials and systems and emphasizes the critical role these technologies play in improving energy storage applications. PV systems are also essential to microgrids, offering dependable, economical, and ecologically friendly power solutions.

1.1. Role of PV in Microgrids

1.1.1. Independent or Supplementary Power Source [3]

- Independent Power Source: PV systems may generate electricity independently using local solar energy in distant locations unrelated to the main power grid.
- Supplemental Power Source: Photovoltaic systems can serve as backup power sources in regions with unreliable power networks, guaranteeing a steady electricity supply even during blackouts.

1.1.2. Enhancing Energy Efficiency [1, 3]

- Energy Complementarity: PV systems can maximize overall efficiency by forming a complementary energy system with other distributed energy resources (such as wind power and energy storage).
- Optimizing Power Dispatch: Microgrids can reduce the fluctuation of PV power output and provide a steady electricity supply by integrating PV systems with energy storage and intelligent control systems.

1.1.3. Increasing System Reliability and Stability [3, 4]

- Island Mode Operation: When the main grid fails, microgrids can transition to island mode, with PV systems providing power for important sectors.
- Rapid Fault Recovery: PV systems can rapidly modify their output to assist in the restoration of power during outages. They can successfully handle system crises in conjunction with other distributed energy sources.

1.1.4. Promoting Renewable Energy Integration [3, 4]

- Encouraging the Integration of Renewable Energy: PV systems enable microgrids to incorporate renewable energy, hence increasing the percentage of clean energy used.
- Environmental Protection: Because photovoltaic systems don't emit greenhouse gasses or other pollutants, they are considered ecologically beneficial.

1.2. Significance of PV

- Sunlight to Electricity Conversion: PV materials and equipment use the photovoltaic effect to transform sunlight into electrical energy, making them a clean and sustainable energy source [3, 4].
- Scalability and Modularity: PV systems are adaptable to different power requirements, ranging from modest residential installations to substantial utility-scale setups [3].
- Environmental Benefits: Photovoltaic (PV) systems provide power free of pollutants and greenhouse gas emissions, promoting sustainability and environmental preservation [3].
- Technological Developments: Ongoing research and development have improved PV systems and materials, boosting durability, cutting prices, and improving efficiency [2].

Photovoltaic PV cells capture solar energy from the sun and convert it to electrical energy, as shown in Figure 1. These solar cells are hooked up in series and parallel to build a massive PV array that delivers the needed voltage and current output levels. The temperature and solar irradiance may be changed to modify the nonlinear features of this PV array.

Each PV panel can function at its highest efficiency, as the manufacturer specifies when the voltage-current practical parameters approach or match the Maximum Power Point (MPP). As the real behaviour of PV panels deviates from ideal circumstances due to the nonlinearity of the I-V characteristics of solar cells, it is essential to estimate the MPP always. PV aging affects the characteristics of the equivalent circuit as well. It might be accomplished using simulation approaches to improve operational efficiency [5].

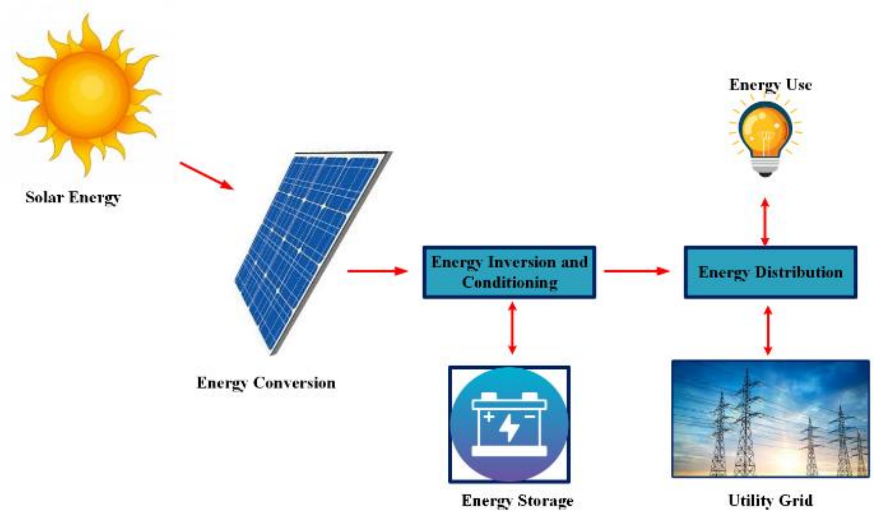

Fig. 1 Solar photovoltaic system [3]

However, the PV panel manufacturer does not give the model characteristics under STC, such as 1000 W/m², 25°C; however, they do provide information on the voltage at the open circuit (V_{oc}), current through a short circuit (I_{sc}), and voltage and current at the point of maximum power (V_{mpp} & I_{mpp}) [6]. The practical parameters fluctuate with every change in weather conditions, and these are retrieved using evolutionary algorithms, numerical approaches, and analytical approaches. Three different ideas are used to predict the overall behaviour of PV devices depending on physical factors. Photovoltaic component modeling is based on the Single Diode Model (SDM), which is followed by the Double Diode Model (DDM), which takes into account recombination loss in the PN junction's depletion region. The Triple Diode Model (TDM) is thought to be a more accurate model than the SDM and DDM. Of those three varieties, single and double-diode photovoltaic variants were utilized most often.

[7] offers a non-iterative method for accurately extracting the five parameters of the single-diode model of solar cells, which improves accuracy and expedites the computation process. This approach dynamically alters key elements of the equation to extract parameters from the I-V curve. The SDM for Photovoltaic (PV) design presented in [8] improves the precision and speed of PV system simulations. This model is effective and useful for PV system designers because it streamlines the intricate nonlinear equations involved. An SDM with five parameters is the simplest and most accurate way to simulate a Photovoltaic (PV) module [9]. Finding a precise set of five distinct equations that nearly resemble the PV module's characteristics as feasible is necessary to solve for these five parameters. The PV module's datasheet has key information on the characteristic curve, which may be used to create the first four equations in the literature. The fifth equation's formulation presents the most obstacles, though. The fifth equation is formulated using a novel analytical technique in [10], producing the most accurate single-diode model.

2. Literature Survey

Several authors explored parameter extraction techniques for Photovoltaic (PV) modeling with the SDM and DDM. Several strategies have been used to increase accuracy and convergence, such as Artificial Intelligence (AI) based approaches and evolutionary algorithms. Here are some discussions on similar works in this field.

[11] provides the Hybridized Arithmetic Operation Algorithm based on Efficient Newton Raphson (HAOA-ENR) to reliably extract parameters of PV models with one or two diodes under varied climatic conditions. This approach surpasses previous methods in improving precision and dependability. An improved differential evolution approach for collecting characteristics from Photovoltaic (PV) cells is proposed in [12]. Compared to current techniques, the method enhances parameter extraction accuracy, reliability, and convergence.

An enhanced technique for determining parameters and calculating PV module performance using a temperature-dependent single-diode model is presented in [13]. To improve accuracy and dependability, this method uses manufacturer datasheet information, which accounts for temperature fluctuations to better forecast PV module performance under various circumstances. A thorough analysis of the interactions between the many electro-devices in PV solar systems, such as controllers, DC-DC boost converters, and PV panels, is given in [14]. It covers their basic concepts, architectural implications, and technical development, emphasising the most recent developments and opportunities for Maximum Power Point Tracking (MPPT) applications. [15] presents a unique approach that uses a generalized Per-Unit Single-Diode Model (PUSDM) to extract PV properties. Numerous PV cells and modules are used to evaluate the approach, which shows good accuracy and minimal computing costs.

[16] focuses on a group of non-iterative parameter extraction strategies and is limited to the single-diode PV model. These methods are usually easy to perform, although they show intermediate accuracy. [17, 18] present comprehensive analytical, numerical, and Genetic Algorithm (GA) approaches for obtaining PV panel characteristics. In order to compare the algorithms, many factors are taken into account: algorithm robustness, calculation speed, accuracy (i.e., how closely the results match experimental data), and simplicity of use [19].

Explicit two-piece quadratic model ETPQM parameters may be extracted using a search-based technique that improves model accuracy over the original explicit equations [20]. An innovative approach is presented to calculate the numerical values of all five parameters while minimizing assumptions and oversimplifications.

The proposed method is based on solving the current-voltage equation for a single diode at five empirically obtained places on the current-voltage curve using the Lambert W-function [21]. The system of non-linear equations is solved using a multi-dimensional NR approach. The Lambert-W function has been used to calculate the Rs and Rsh values on the solar panel at various light intensity levels [22]. In reference [23], a comparative MPPT study is done for the Perturbs and Observe (P&O), incremental conductance IC, and Modified Regula Falsi Method (MRFM).

A precise numerical approach for determining single-diode model parameters is provided in the literature [23, 24], and [25]. This reference offers a precise numerical method for obtaining single-diode model parameters. The linear least squares approach in reference [26] has been used to solve three linear equations that describe the shunt resistance, saturation current, and photocurrent as functions of the ideality factor and series resistance. Minimizing parasitic resistive losses is the last prerequisite for designing a solar cell with high efficiency. To enhance solar cell efficiency, the series resistance, which is determined by the emitter resistance and top contact design, must be properly tuned for each kind and size of solar cell structure [27]. To ascertain the parameters of the nonlinear I–V equation, the main objective is to alter the curve at the Open Circuit (OC), Maximum Power (MP), and Short Circuit (SC) points. It also considers the influence of series and parallel resistances, ensuring that the model's maximum power matches the maximum power of the actual array [28, 29]. In order to improve the power-generating efficiency of Photovoltaic (PV) solar systems, [30] compares the SDM and DDM of PV solar cells. The current/voltage (IV) characteristics of Si-crystalline PV modules under non-standard irradiation and temperature conditions are evaluated in this work using SDM and DDM. Using the Chaibi and Ishaque techniques, the parameters of each equivalent-circuit model are determined [31]. The fifth equation, which considers the specific without needing any approximations, is precisely given in [32]. Numerous Single Diode Model (SDM) techniques have been put out in the literature, and each has unique benefits regarding accuracy, computing complexity, and convergence stability. To place the suggested study within the present research environment, Table 1 lists the advantages and disadvantages of the SDM techniques that are currently in use.

Table 1. Comparative summary of Single Diode Model (SDM) approaches, highlighting their advantages, disadvantages

S.No	Methodology	Advantages	Disadvantages	Ref
1	Hybrid Bird Mating Optimizer (BMO) with Lambert W-function	High precision and efficient parameter estimation	Implementation complexity of hybrid algorithms	[34]
2	Lightning Attachment Procedure Optimization (LAPO)	High accuracy that works well in unpredictable situations	Intensive computation that needs to be adjusted	[35]
3	Particle Swarm Optimization (PSO)	Strong capacity to search globally	Slow convergence	[36]
4	Villalva Analytical Method	High accuracy, low computational cost	Needs an initial guess	[28]
5	Lambert W-Function Analytical Approach	Quick and precise	Initial condition sensitivity	[37]
6	Genetic Algorithm	Robust under varying conditions	Expensive computational cost	[38]
7	Artificial Neural Network	Ability to adjust to nonlinearities	Requires large training data	[39]

Research on Photovoltaic (PV) systems in real-time is more challenging than with other sources as it requires an accurate PV emulator that can mimic the nonlinear properties of a PV cell. PV Investigators have created a variety of emulators using different setups. [33] discusses various PV emulator topologies along with an extensive evaluation of each technique, with special attention paid to its accuracy, level of difficulty, implementation cost, sensitivity to changing conditions in the environment, hardware deployment, and efficiency.

Photovoltaic (PV) systems are gaining popularity as clean and sustainable energy sources due to their capacity to reduce reliance on fossil fuels and cut carbon emissions. Designing effective Maximum Power Point Tracking (MPPT) algorithms and forecasting energy generation under various climatic circumstances depend on accurate PV system modelling. A flexible and dependable PV model is required throughout the design phase to increase the performance and operational stability of PV systems.

Even with great advancements in PV modeling, it is still difficult to precisely extract the properties of PV cells under various irradiation and temperature circumstances. The speed, accuracy, and consistency of convergence of existing parameter extraction techniques, such as analytical and numerical methods, across various solar panel types are frequently limited. Furthermore, there is a knowledge vacuum about how these approaches work with more recent technologies like PERC, Topcon, HJT, and Kaneka solar cells because the majority of comparative research has concentrated on monocrystalline and polycrystalline panels. This study addresses these shortcomings by focusing on the mathematical modeling of the SDM and the extraction of five crucial parameters under reference and generic conditions utilizing two distinct techniques, namely virtual and numerical.

In contrast to earlier research, this study compares six distinct types of solar panels in detail and uses experimental data from a Chroma PV Emulator (62000H-S Series) to confirm the derived characteristics. With an MPPT efficiency of 98.78%, the findings show that Villalva's technique outperforms numerical methods in terms of consistency and dependability, achieving greater precision and tighter alignment with hardware results. Particularly for contemporary PV technology, this study provides deeper insights into enhancing the accuracy of parameter extraction and PV system modelling. The structure of the paper is as follows. A preamble on the PV system's modeling is discussed in Section 3. Section 4 addresses parameter extraction under general and reference settings, which include the several models employed in this research. The findings obtained are discussed in Section 5, along with a comparison to the experimental results. Lastly, the major findings are summarized in Section 6.

3. Mathematical Modeling of Solar PV Cell

For PV analysis, the SDM is better than the DDM as it requires fewer parameters and has lower processing costs, facilitating extraction and increasing convergence in dynamic environments. The SDM is more suited for real-time tracking and control because it balances precision and simplicity, even though the DDM can account for both diffusion and recombination losses. It faithfully replicates the output properties of various PV modules and cells under a range of climate conditions [32]. SDM consists of an anti-parallel diode and current source connected in series and parallel at the diode's terminal by a resistor [17, 19, 40, 41]. By applying Kirchhoff's law and Shockley's diode equation to the analogous circuit shown in Figure 2, the mathematical formula for the current produced in the PV cell at a certain operating voltage may be obtained.

The current-voltage relationship of photovoltaic cells is as follows:

$$I = I_{pv} - I_d - I_p \tag{1}$$

The Equation (1) indicates the fundamental connection between current and voltage in a photovoltaic cell. Where I_{pv} represents the light-generated current, the diode current by I_d, and the shunt current by I_p. General I-V characteristics of a PV cell are expressed through Equation (2).

It offers a realistic simulation and analysis of photovoltaic cells nonlinear behaviour while accounting for the effects of shunt and series resistance.

$$I = I_{pv} - I_o\left(e^{\left(\frac{V+R_sI}{V_t}\right)} - 1\right) - \frac{V+R_sI}{R_p} \tag{2}$$

Where R_s and R_p stand for the parasitic series and shunt resistance, I_{pv} for the light-generated current, I_o for the diode reverse saturation current, and n for the diode ideality constant respectively, these are the five parameters to be retrieved.

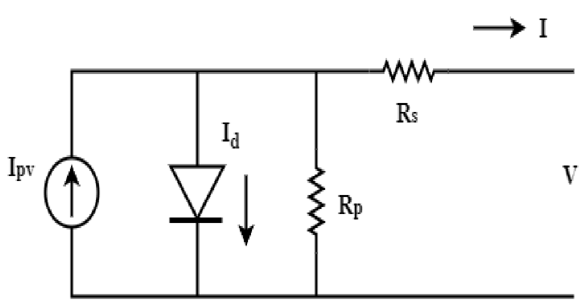

Fig. 2 Equivalent circuit of SDM solar cell [17, 19]

The diode thermal voltage is determined by:

$$V_t = \frac{nkT}{q} \tag{3}$$

In Equation (3), T is the temperature in Kelvin, q is the electron charge (1.602176487*10−19), and k is Boltzmann's constant (1.3806504 * 10−23). It draws attention to the diode's behavior's temperature dependency, essential for comprehending and forecasting PV cell performance in various environmental settings. The quintet of unidentified parameters I_{pv}, I_o, n, R_s, R_p are not given by the manufacturers, and they supply just V_{mp}, V_{oc}, I_{mp}, I_{sc}, K_v, K_i under STC (25°C, 1000 W/m^2). Three steps must be followed to assess the performance of solar PV modules: 5-parameter extraction at STC, modifying the 5-parameters to the necessary environmental conditions and computing the I–V equation for the solar PV cell. The following sections examine the methods.

4. Method of Parameters Extraction

The photovoltaic parameters must be retrieved by solving nonlinear equations generated from the electrical models. The solar cell's parameter extraction is a highly nonlinear and challenging optimization issue. In the following subsection, the formulation of mathematical equations for numerical and villalva methods is explained. At standard test conditions, the parameters are designed as reference values. Meanwhile, the parameters are estimated at other temperatures using mathematical equations of general conditions.

4.1. Role of PV in Microgrids

Based on SDM, the I-V relation is represented by Equation (2) in the following way under the reference conditions, which are set standards for PV cell testing and comparison.

$$I = I_{pvref} - I_{oref}\left(e^{\left(\frac{V+R_{sref}I}{V_{tref}}\right)} - 1\right) - \frac{V+R_{sref}I}{R_{pref}} \tag{4}$$

This Equation (4) makes it possible to compare and choose the best parts for microgrid applications by allowing the performance of various PV cells and systems to be benchmarked.

The diode ideality factor under reference condition is:

$$n_{ref} = \frac{V_{tref}q}{KT_{ref}} \tag{5}$$

Equation (5) is an important metric for describing the performance of photovoltaic cells, and this equation finds the diode ideality factor under reference conditions.

The modeling approach of solar PV cells starts with acquiring data from the manufacturer's data sheet and then solving Equation (4). As the I-V equations are the functions of five unknowns, five independent equations are necessary. Equation (4) yields Equations (6), (8), and (14) when the conditions for maximum power point, open circuit, and short circuit are used. Similarly, by differentiating the solar cell's power and current values with respect to voltage, Equations (7), (9), and (15) are obtained. At short circuit condition: $I=I_{sc}$, $V=0$

$$I_{scref} = I_{pvref} - I_{oref}\left(e^{\left(\frac{R_{sref}\, I_{scref}}{V_{tref}}\right)} - 1\right) - R_{sref}\frac{I_{scref}}{R_{pref}} \quad (6)$$

Equation (6) assists in calculating the PV cell's short circuit current (I_{sc}), a critical measure for assessing the cell's performance under situations of maximum irradiation. Equation (4) determines the series resistance R_{pref}, which influences the PV cell's efficiency,

$$\left.\frac{dI}{dV}\right|_{I=I_{scref}, V=0} = -\frac{1}{R_{pref}} \quad (7)$$

At open circuit condition: $V= V_{oc}$, $I=0$

$$I_{pvref} - I_{oref}\left(e^{\left(\frac{V_{ocref}}{V_{tref}}\right)} - 1\right) - \frac{V_{ocref}}{R_{pref}} = 0 \quad (8)$$

Equation (8) assists in identifying the open circuit voltage (V_{oc}), an additional crucial characteristic for evaluating the highest voltage a photovoltaic cell can produce. Under STC, Equation (4) equals the series resistance $R_{sref,}$ which affects the PV cell's total efficiency and voltage drop.

$$\left.\frac{dI}{dV}\right|_{I=0,\, V=V_{ocref}} = -\frac{1}{R_{sref}} \quad (9)$$

The open circuit voltage is used in this Equation (10) to determine the photo-generated current (I_{pvref}). It's crucial to comprehend how much current the PV cell generates under typical test conditions.

$$I_{pvref} = I_{oref}\left(e^{\left(\frac{V_{ocref}}{V_{tref}}\right)} - 1\right) - \frac{V_{ocref}}{R_{pvref}} \quad (10)$$

Substituting Equation (10) into Equation (6) gives the expression for I_{scref},

$$I_{scref} = I_{oref}\left(e^{\left(\frac{V_{ocref}}{V_{tref}}\right)} - e^{\left(\frac{R_{sref}\, I_{scref}}{V_{tref}}\right)}\right) + \frac{V_{ocref} - I_{scref}\, R_{sref}}{R_{pref}} \quad (11)$$

By simplifying Equation (11), the following expression is obtained:

$$I_{scref} = I_{oref}\left(e^{\left(\frac{V_{ocref}}{V_{tref}}\right)}\right) + \frac{V_{ocref} - I_{scref}\, R_{sref}}{R_{pref}} \quad (12)$$

An elaborate expression for the short circuit current (I_{scref}) may be found in these Equations (11) and (12). Through the consideration of many characteristics, such as series resistance and photo-generated current, they are utilized to improve the computation of (I_{sc}). The above expression is resolved for obtaining reverse saturation current I_{oref}, which is essential for understanding the leakage current in the PV cell. It affects the cell's overall effectiveness and function.

$$I_{oref} = \left(I_{scref} - \frac{V_{ocref} - I_{scref}\, R_{sref}}{R_{pref}}\right) e^{\left(-\frac{V_{ocref}}{V_{tref}}\right)} \quad (13)$$

At maximum power point condition: $V=V_m$, $I=I_m$

$$I_{mref} = I_{pvref} - I_{oref}\left(e^{\left(\frac{V_{mref} + R_{sref}\, I_{mref}}{V_{tref}}\right)} 1\right) - \frac{V_{mref} + R_{sref}\, I_{mref}}{R_{pref}} \quad (14)$$

At MPP, the current is represented by Equation (14), ($V = V_m$, $I = I_m$). It is essential for figuring out the PV cell's maximum power output, which is a crucial performance indicator. The derivative of power concerning voltage at MPP in Equation (4) is equal to zero under STC and may be found using the following formula:

$$\left.\frac{dP}{dV}\right|_{I=I_{mref}, V=V_{mref}} = 0 \quad (15)$$

In order to optimize the power production and improve the performance of the PV system, Equation (15) is employed. Where V_{ocref} is the open circuit voltage at STC, I_{scref} is the short circuit current at STC, I_{mref} is the current at MPP, and V_{mref} is the voltage at MPP at STC. Expression for I_{mref} is obtained by substituting Equations (13) and (10) in Equation (14), which uses multiple parameters to compute. It aids in precisely figuring out the PV cell's maximum power output.

$$I_{mref} = I_{oref} - \frac{V_{mref} + R_{sref}\, I_{mref} - R_{sref}\, I_{scref}}{R_{pref}} - \left(I_{oref} - \frac{V_{ocref} - R_{sref}\, I_{scref}}{R_{pref}}\right)\left(e^{\left(\frac{V_{mref} + R_{sref}\, I_{mref}}{V_{tref}}\right)}\right) \quad (16)$$

To make sure that the power output is maximized at MPP, this equation rewrites the power derivative statement. It is essential for guaranteeing effective energy conversion and maximizing the performance of the PV system.

$$\left.\frac{dP}{dV}\right|_{\substack{I=I_{mref} \\ V=V_{mref}}} = \frac{d(IV)}{dV} = I + \frac{dI}{dV}V = 0 \quad (17)$$

The original Equation (4) cannot be solved analytically since it is transcendental. Rewriting it as Equation (18) enables the use of numerical techniques to accurately calculate current and voltage in PV cells under a variety of conditions.

$$I = f(I, V) \quad (18)$$

Differentiating Equation (18) gives:

$$\mathrm{dI} = \mathrm{df(I,V)} = \mathrm{dI}\frac{\partial \mathrm{f(I,V)}}{\partial \mathrm{I}} + \mathrm{dV}\frac{\partial \mathrm{f(I,V)}}{\partial \mathrm{V}} \tag{19}$$

Differentiating the numerical statement allows us to see how modest changes in voltage affect current. This is essential for examining the dynamic behavior of photovoltaic cells and enhancing their efficiency.

Consequently, the rate of change of current concerning voltage is provided by this equation (20), which is crucial for figuring out the PV cell's electrical properties. It improves understanding of how the cell reacts to modifications in operating conditions.

$$\frac{\mathrm{dI}}{\mathrm{dV}} = \frac{\frac{\partial \mathrm{f(I,V)}}{\partial \mathrm{V}}}{1-\frac{\partial \mathrm{f(I,V)}}{\partial \mathrm{I}}} \tag{20}$$

Equations (20), (17), gives us:

$$\left.\frac{\mathrm{dP}}{\mathrm{dV}}\right|_{\substack{\mathrm{I=I_{mref}}\\ \mathrm{V=V_{mref}}}} = \frac{\mathrm{d(IV)}}{\mathrm{dV}} = \mathrm{I_{mref}} + \frac{\frac{\partial \mathrm{f(I,V)}}{\partial \mathrm{V}}}{1-\frac{\partial \mathrm{f(I,V)}}{\partial \mathrm{I}}}\mathrm{V_{mref}} \tag{21}$$

This Equation (21) is employed to guarantee that the PV system maximizes power generation by operating at its best. This comprehensive Equation (22) aids in precisely computing the power derivative at MPP while taking into account a number of variables, including reverse saturation current and series resistance. It is essential for optimizing the PV system's efficiency.

From above:

$$\left.\frac{\mathrm{dP}}{\mathrm{dV}}\right|_{\substack{\mathrm{I=I_{mref}}\\ \mathrm{V=V_{mref}}}} = \mathrm{I_{mref}} + \mathrm{V_{mref}}\left(\frac{-\frac{\left(\mathrm{I_{oref}}-\frac{\mathrm{V_{oref}}-\mathrm{R_{sref}}\mathrm{I_{scref}}}{\mathrm{R_{pref}}}\right)e^{\left(\frac{\mathrm{V_{mref}}+\mathrm{R_{sref}}\mathrm{I_{mref}}}{\mathrm{V_{tref}}}\right)}}{\mathrm{V_{tref}}\mathrm{R_{pref}}}-\frac{1}{\mathrm{R_{pref}}}}{1+\frac{\left(\mathrm{I_{oref}}-\frac{\mathrm{V_{oref}}-\mathrm{R_{sref}}\mathrm{I_{scref}}}{\mathrm{R_{pref}}}\right)e^{\left(\frac{\mathrm{V_{mref}}+\mathrm{R_{sref}}\mathrm{I_{mref}}}{\mathrm{V_{tref}}}\right)}}{\mathrm{V_{tref}}\mathrm{R_{pref}}}-\frac{\mathrm{R_{sref}}}{\mathrm{R_{pref}}}}\right) \tag{22}$$

Together with other Equations (7), (21) and (22), this Equation (23) creates a system of equations that contains unknown parameters like n_{ref}, R_{pref}, and R_{sref}. It is important to solve this system to model the behaviour of the PV cell precisely.

$$-\frac{1}{\mathrm{R_s}} = \left(\frac{-\frac{\left(\mathrm{I_{oref}}-\frac{\mathrm{V_{oref}}-\mathrm{R_{sref}}\mathrm{I_{scref}}}{\mathrm{R_{pref}}}\right)e^{\left(\frac{\mathrm{V_{mref}}+\mathrm{R_{sref}}\mathrm{I_{mref}}}{\mathrm{V_{tref}}}\right)}}{\mathrm{V_{tref}}\mathrm{R_{pref}}}-\frac{1}{\mathrm{R_{pref}}}}{1+\frac{\left(\mathrm{I_{oref}}-\frac{\mathrm{V_{oref}}-\mathrm{R_{sref}}\mathrm{I_{scref}}}{\mathrm{R_{pref}}}\right)e^{\left(\frac{\mathrm{V_{mref}}+\mathrm{R_{sref}}\mathrm{I_{mref}}}{\mathrm{V_{tref}}}\right)}}{\mathrm{V_{tref}}\mathrm{R_{pref}}}-\frac{\mathrm{R_{sref}}}{\mathrm{R_{pref}}}}\right) \tag{23}$$

The five unknown parameters I_{pvref}, I_{oref}, n_{ref}, R_{sref} and R_{pref} now be found using Equations ((10), (12), (16), (22) and (23)). The simplicity and quick convergence of the Newton-Raphson approach made it a popular choice for iterative computer applications, as well as for figuring out the roots of implicit transcendental equations.

Based on the first suggested values, the Newton-Raphson technique was used in this study to solve the five equations produced. The iterations proceeded until the difference between the estimated and empirically obtained powers was less than this value.

For numerical solutions, choosing a suitable initial value is essential. While doing these computations, the data sheet's values were the only ones utilized as a starting point.

As a result, the starting values ought very closely to approximate the actual values. To begin with, a very low tolerance value is established, and the starting values for the series and shunt resistances are set.

In this part, the previously generated Equations (10), (12), (16), (22) and (23) were used to compute the values of the I_{pvref}, I_{oref}, n_{ref}, R_{sref} and R_{pref} parameters. The PV module's five parameters may be grouped in the following matrix form in that order:

$$\mathrm{x} = \begin{bmatrix} \mathrm{I_{pvref}} \\ \mathrm{I_{oref}} \\ \mathrm{n_{ref}} \\ \mathrm{R_{sref}} \\ \mathrm{R_{pref}} \end{bmatrix}, \mathrm{F(x)} = \begin{bmatrix} \mathrm{f_1} \\ \mathrm{f_2} \\ \mathrm{f_3} \\ \mathrm{f_4} \\ \mathrm{f_5} \end{bmatrix} \tag{24}$$

The 5 parameters of an SDM are estimated by solving F(x) numerically using the Newton-Raphson method. This method is essential for managing complicated PV models. Where F(x) is the array of five Equations (10), (12), (16), (22) and (23) as shown in Equation (24).

The partial derivatives of the system of equations with respect to the parameters are represented by the Jacobian matrix J(x). It is employed in the Newton-Raphson technique to solve for the parameters in an iterative manner, guaranteeing convergence to the right values.

$$\mathrm{J(x)} = \begin{bmatrix} \frac{\partial \mathrm{f_1}}{\partial \mathrm{I_{pvref}}} & \frac{\partial \mathrm{f_1}}{\partial \mathrm{I_{oref}}} & \frac{\partial \mathrm{f_1}}{\partial \mathrm{n_{ref}}} & \frac{\partial \mathrm{f_1}}{\partial \mathrm{R_{sref}}} & \frac{\partial \mathrm{f_1}}{\partial \mathrm{R_{pref}}} \\ \frac{\partial \mathrm{f_2}}{\partial \mathrm{I_{pvref}}} & \frac{\partial \mathrm{f_2}}{\partial \mathrm{I_{oref}}} & \frac{\partial \mathrm{f_2}}{\partial \mathrm{n_{ref}}} & \frac{\partial \mathrm{f_2}}{\partial \mathrm{R_{sref}}} & \frac{\partial \mathrm{f_2}}{\partial \mathrm{R_{pref}}} \\ \frac{\partial \mathrm{f_3}}{\partial \mathrm{I_{pvref}}} & \frac{\partial \mathrm{f_3}}{\partial \mathrm{I_{oref}}} & \frac{\partial \mathrm{f_3}}{\partial \mathrm{n_{ref}}} & \frac{\partial \mathrm{f_3}}{\partial \mathrm{R_{sref}}} & \frac{\partial \mathrm{f_3}}{\partial \mathrm{R_{pref}}} \\ \frac{\partial \mathrm{f_4}}{\partial \mathrm{I_{pvref}}} & \frac{\partial \mathrm{f_4}}{\partial \mathrm{I_{oref}}} & \frac{\partial \mathrm{f_4}}{\partial \mathrm{n_{ref}}} & \frac{\partial \mathrm{f_4}}{\partial \mathrm{R_{sref}}} & \frac{\partial \mathrm{f_4}}{\partial \mathrm{R_{pref}}} \\ \frac{\partial \mathrm{f_5}}{\partial \mathrm{I_{pvref}}} & \frac{\partial \mathrm{f_5}}{\partial \mathrm{I_{oref}}} & \frac{\partial \mathrm{f_5}}{\partial \mathrm{n_{ref}}} & \frac{\partial \mathrm{f_5}}{\partial \mathrm{R_{sref}}} & \frac{\partial \mathrm{f_5}}{\partial \mathrm{R_{pref}}} \end{bmatrix} \tag{25}$$

The incremental change in the unknown parameters during each Newton-Raphson technique iteration is computed using this Equation (26). It is necessary to improve the parameter estimations and provide precise outcomes.

$$y_i = -J^{-1}F(x_i) \tag{26}$$

To ensure that the solution converges to the right values, this Equation (27) modifies the parameter estimations throughout each iteration. High precision is ensured by continuing the iterative procedure until the result satisfies the given tolerance.

$$x_{i+1} = x_i + y_i \tag{27}$$

Where x_{i+1} is the input to the next iteration, the iteration continued until $F(x) \leq$ tol. Here, tolerance is $1e^{-10}$.

4.2. Numerical Method at General Condition

The solar system's I-V characteristics characterize its static behavior at set temperatures and irradiance levels. When the two crucial components are gradually changed over an extended length of time, the system's dynamic behavior may be considered; the current is assessed as a function of time. The following formulas provide the values of the five primary parameters (I_{pv}, I_o, n, R_s and R_p) at other temperatures and irradiance using the five values calculated at reference conditions.

- The light-generated current (I_{pv}):

$$I_{pv} = (G/G_{ref})\left(I_{pvref} + K_i(T - T_{ref})\right) \tag{28}$$

Where K_i is the short circuit temperature coefficient(A/°C), G is solar irradiance at real conditions (W/m^2), and G_{ref} is solar irradiance at standard test conditions (W/m^2). This Equation (28) uses the actual solar irradiance (G) and temperature (T) to determine the light-generated current (I_{pv}). It modifies the reference current (I_{pvref}) to reflect variations in temperature and irradiance in real-world circumstances. This is essential for forecasting PV module performance in different conditions.

- The diode reverse saturation current (Io):

$$I_o = I_{oref}(T/T_{ref})^3 e^{\left(\frac{V_{gap} N_s}{V_{tref}\left(1-\frac{T_{ref}}{T}\right)}\right)} \tag{29}$$

where T_{ref} and T are the reference and cell temperatures, V_{gap} is the semiconductor band gap energy, and the PV module's solar cell count is denoted by N_s. This Equation (29) calculates the diode reverse saturation current (I_o), which is temperature-dependent. It takes into account the semiconductor band gap energy (V_{gap}) and the number of solar cells (N_s). This parameter is crucial for determining the leakage current in the PV cell since it influences overall efficiency and performance.

- The diode ideality constant in terms of thermal voltage Vt, connects the thermal voltage (Vt) with the cell temperature (T). The diode ideality constant (n) is critical for precisely simulating the PV cell's I-V properties, which are temperature sensitive.

$$V_t = V_{tref}(T/T_{ref}) \tag{30}$$

- Series resistance (Rs), which influences voltage drop and overall efficiency. It includes the thermal voltage and reverse saturation current into account while adjusting the reference series resistance (Rsref) for actual circumstances.

$$R_s = R_{sref} - \left[\left(\frac{V_t}{I_o}\right) e^{(-V_{oc}/V_t)}\right] \tag{31}$$

Where V_{oc} is the open circuit voltage.

- Shunt Resistance (Rp) creates a route for leakage current. It modifies the reference shunt resistance (Rpref) according to the reference and actual irradiance levels. Shunt resistance affects the PV module's efficiency and fill factor.

$$R_p = R_{pref}(G_{ref}/G) \tag{32}$$

At any operating point, expressions for V_{oc} and I_{sc} are given as:

$$V_{oc} = V_{ocref} - K_v(T_{ref} - T) + V_t \ln(G/G_{ref}) \tag{33}$$

$$I_{sc} = I_{scref}(G/G_{ref}) + K_i(T - T_{ref}) \tag{34}$$

Equation (33) determines the open circuit voltage (V_{oc}) for various irradiance and temperature ranges. The temperature coefficient (K_v) and the natural logarithm of the irradiance ratio are considered when adjusting the reference open circuit voltage (V_{ocref}) for actual conditions. The Equation (34) calculates the short circuit current (I_{sc}) depending on irradiance and temperature. It adjusts the reference short circuit current (I_{scref}) for real-world conditions, taking into account the temperature coefficient (K_i). This value is required to determine the maximum current the PV module can generate. Based on the actual irradiance, Equation (35) determines the current at the maximum power point (I_m). It modifies the reference current at MPP (I_{mref}) to account for environmental factors.

$$I_m = I_{mref}(G/G_{ref}) \tag{35}$$

The voltage at the maximum power point (V_m) at various temperatures might be determined through Equation (36). In order to adjust the reference voltage at MPP (V_{mref}) for the actual conditions, it considers the temperature coefficient (K_v). In order to maximize the PV module's power production, this value is crucial.

$$V_m = V_{mref} - K_v(T_{ref} - T) \tag{36}$$

Equation (37) calculates the power at the MPP (P_m) by multiplying the voltage and current at the MPP. It gives a clear indication of the maximum power a PV module can generate under specific conditions, which is essential for system design and performance assessment.

$$P_m = I_m V_m \tag{37}$$

4.3. Villalva Method

The Solar PV device's I-V characteristic is determined by its internal parameters (R_s, R_p) and external factors like temperature and irradiation intensity. The quantity of incident light directly impacts the charge carrier production process and, in turn, the device's current generation.

The I_{scref}, which is the highest current that may be drawn at the terminals of a practical device, is the only current that is included in datasheets.

Since the parallel resistance is usually large and the series resistance is low in real-world devices, the assumption $I_{sc} = I_{pv}$ is often employed when modeling PV devices. Equation (28) describes how the light-generated current of the PV cell is affected by temperature and solar irradiation linearly. The expression for reference saturation current is expressed as:

$$I_{oref} = \frac{I_{scref}}{\exp\left(\frac{V_{ocref}}{V_{tref}}\right) - 1} \tag{38}$$

Using the short circuit current (I_{scref}) and open circuit voltage (V_{ocref}), Equation (38) determines the reference saturation current (I_{oref}). It occurs under open-circuit circumstances and is essential for figuring out the PV cell's leakage current, which impacts the device's overall performance and efficiency.

As the reference [32] stated, the experimental data is used to indirectly determine the reference saturation current I_{oref} via Equation (38), where $V = V_{ocref}$, $I = 0$, and $I_{pv} = I_{scref}$.

$$I_o = \frac{I_{scref} + K_i(T - T_{ref})}{\exp((V_{ocref} + K_v(T - T_{ref}))/V_t) - 1} \tag{39}$$

This Equation (39) considers temperature while calculating the saturation current (I_o). Both the thermal voltage (V_t) and the temperature coefficients (K_i and K_v) are included. To precisely predict the behavior of the PV cell at various temperatures, this modification is necessary.

Equation (39) is created by adding the voltage and current coefficients, K_i and K_v, to Equation (38). Since the saturation current I_o is highly temperature-dependent, Equation (39) suggests an alternative method of expressing this dependence. The model's maximum power ($P_{m,m}$) and the experimental maximum power ($P_{m,e}$) are equal at MPP. This indicates that there is only one pair R_s, R_p that ensures $P_{m,m} = P_{m,e}$, at the ($V_{mp}I_{mp}$) point of the I-V curve. Based on these data, a strategy for modifying R_s and R_p is proposed in the reference [28] study.

The relationship between R_s and R_p, the two unknowns in Equation (2), may be found using the formula $P_{m,m} = P_{m,e}$. The following is the solution to the resulting equation for R_s.

$$P_{m,m} = V_m \left\{ I_{pv} - I_0 \left[\exp\left[\frac{(V_m + I_m R_s)}{N_s a}\right] - 1 \right] - \frac{V_m + R_s I_m}{R_p} \right\} = P_{m,e} \tag{40}$$

Equation (40) ensures that the experimental maximum power point ($P_{m,e}$) and the mathematical model coincide, which is necessary to optimize the PV system's performance.

$$R_p = \frac{V_m(V_m + I_m R_s)}{V_m I_{pv} - V_m I_0 \exp\left[\frac{(V_m + I_m R_s)}{N_s a}\frac{q}{kT}\right] + V_m I_0 - P_{m,e}} \tag{41}$$

Equation (41) states that for any value of Rs, there is a value of Rp such that the experimental point is crossed by the mathematical I-V curve. It is possible to further improve the existing model by using the iterative solution of Rs and Rp.

In order to get the optimum model solution, each iteration changes Rs and Rp; thus, Equation (42) could be added to the model, which offers an initial estimate for the iterative solution.

$$I_{pvref} = \frac{R_p + R_s}{R_p} I_{scref} \tag{42}$$

Based on the maximum power point current (I_{mp}) and the short circuit current (I_{scref}), Equation (43) generates the initial value for the shunt resistance ($R_{p,\,min}$). It ensures that the model converges to an exact answer by acting as the beginning point for the iterative process.

$$R_{p,min} = \frac{V_{mp}}{I_{scref} - I_{mp}} - \frac{V_{ocref} - V_{mp}}{I_{mp}} \tag{43}$$

5. Simulation and Experimental Results

In MATLAB, the mathematical equations (formulated in section 4) are solved by programming the MATLAB codes. The manufacturer's data sheet parameters are used to carry out computations. The input parameters from six different datasheets are listed in Table 2. The typical sun radiation is 1000 W/m^2, and the cell temperature is 25°C. Each of the six types of PV cells (monocrystalline, polycrystalline, PERC, TOPCon, HJT, and Kaneka) is simulated using both the numerical and Villalva approaches.

Table 2. Six different datasheets of solar PV cells [42-47]

Panel Parameters	Mono Crystalline	Poly Crystalline	PERC	TOPCon	HJT	Kaneka
P_{max}	120	120	145	124	100	100
V_{mp}	19.28	18.72	23.08	18.6	19.8	54
I_{mp}	6.22	6.47	6.28	6.66	5.05	1.87
V_{oc}	22.68	22.68	27.58	21.9	22.9	71
I_{sc}	6.66	6.92	6.8	7.33	5.45	2.25
K_v (V/°C)	-0.3	-0.3	-0.28	-0.28	-0.227	-0. 39
K_i (A/°C)	0.06	0.06	0.05	0.008	0.031	0.056
N_s	36	36	40	124	33	106

Table 3. Parameter extraction of different types of solar PV cell

Types of Solar PV Cell	Methods	Parameter Extraction				
		I_{pv}	I_o	N	R_s	R_p
Mono Crystalline	A	6.66	1.51e^{-10}	1	0.08	127.68
	B	6.66	8.67 e^{-10}	0.86602	3.28 e^{-10}	55.046
	C	6.6648	1.97 e^{-10}	0.8512	3.98 e^{-10}	55.046
Poly Crystalline	A	6.93	1.57 e^{-10}	1	0.18	163.98
	B	6.92	2.00 e^{-10}	1.07	6.46 e^{-10}	56.634
	C	6.925	2.59 e^{-10}	1.0517	7.86 e^{-10}	56.634
PERC	A	6.81	1.521 e^{-10}	1	0.19	92.87
	B	6.8	1.8078 e^{-10}	1.0614	5.0499 e^{-10}	55.21
	C	6.8041	3.12 e^{-10}	1.0432	6.14 e^{-10}	55.21
TOPCon	A	7.34	3.856 e^{-10}	1	0. 58.50205	49.91
	B	7.33	8.9163 e^{-10}	0.83522	1.1988 e^{-10}	32.235
	C	7.3307	2.26 e^{-10}	0.82093	1.46 e^{-10}	32.235
HJT	A	5.45	1.025 e^{-10}	1	0.05	94.33
	B	5.45	9.8516 e^{-10}	0.82896	4.7988 e^{-10}	58.502
	C	5.452	1.94 e^{-10}	0.82093	5.83 e^{-10}	58.502
Kaneka	A	2.3	1.08 e^{-10}	1	4.45	182.31
	B	2.2501	1.42 e^{-10}	1.7303	0.0080682	163.36
	C	2.2515	0.0001291	1.7007	0.0098041	163.36
A- Villalva approach, B- Numerical approach reference condition, C- Numerical approach general condition at 45°C						

Six different kinds of solar cells are used in this study to allow for a thorough performance comparison under various circumstances. Monocrystalline cells are more costly yet have a long lifespan and good efficiency (15-22%). Although polycrystalline cells are significantly less efficient (13%-18%), they are more affordable. PERC cells increase efficiency by lowering electron recombination through a rear passivation layer. TOPCon cells use a tunnel oxide layer and passivated contact to increase efficiency by up to 24%. High efficiency (up to 25%) and improved temperature tolerance are achieved by HJT cells, which mix crystalline and thin-film silicon. Although Kaneka cells, which are composed of amorphous silicon, are flexible and lightweight, their efficiency is only 10% to 12%. This wide range of choices makes it possible to comprehensively assess material qualities, effectiveness, and environmental impact.

The simulations take the known parameters from the datasheets as inputs, and the unknown values are adjusted iteratively to get the best match with the experimental results. Table 3 lists the five unknown parameters' computed values for each kind of PV cell based on the outcomes of these simulations. This thorough analysis makes a thorough comparison of the performance traits of various PV technologies possible.

The simulation results are compared using a solar PV emulator (62000HS Series). The standalone unit's integrated EN50530/Sandia SAS I-V model without a PC controller may quickly program the Vmp, Imp, Voc, and Isc parameters for I-V curve simulation. During the static MPPT performance test, the user has the option to activate the data recording feature on the soft panel.

The remote controller or the front panel keypad may be used to easily manage the DC power supply of the 62000H-S Series via Ethernet, USB, RS232, RS485, GPIB, or APG. The model 62000H-S Series has a graphical user interface software via remote digital interface (USB, GPIB, Ethernet, or RS232) control. The Chroma solar emulator is provided with a Sandia Excel sheet. Feeding the panel data into Sandia Excel, I-V/P-V curves are produced. This makes it simple to customize the I-V curve of the 62000H-S Series and the P-V and I-V curves for real-time testing. The I-V curve output of a real solar array is affected by a number of meteorological factors, including temperature, precipitation, irradiance, and shading from clouds or trees.

5.1. Simulation Results

Table 2 offers data sheets for six different types of solar PV cells that are monocrystalline [42], polycrystalline [43], PERC [44], Topcon [45], HJT [46], and Kaneka [47]. The data sets contain the following parameters: number of cells in series (N_s), temperature coefficient for voltage (K_v (V/°C)), temperature coefficient for current (K_i (A/°C)), open circuit voltage (V_{oc}), short circuit current (I_{sc}), maximum power point (Pmax), voltage at maximum power point (V_{mp}), and current at maximum power point (I_{mp}). Even if the PV cells in Table 2 have similar capacities, there are a few reasons for the variation in cell parameters, like material differences, technological variations, temperature coefficients, manufacturing tolerances and irradiance responses, which lead them to differ in terms of performance. Two methodologies are employed to obtain the parameters under standard test circumstances.

The extracted parameters are used to plot panel characteristics curves. Figure 3 shows the I-V and P-V characteristics of six solar panels under STC. From Figure 3, it is clear that villalva closely matches experimental compared to numerical methods. It is also to be noted that the panel characteristic curves obtained in the Sandia sheet (denoted as experimental Sandia) closely match the simulation plot.

5.2. Experimental Results

To validate the extracted parameters obtained from the two mathematical approaches, the simulation outcomes are compared with experimental outputs. In the experimentation, a chroma PV emulator is used to carry out a practical test. Table 4 shows the specifications of chroma PV emulation. In this experiment, the MPPT control and converter interfaces are not designed. As a result, the load is directly linked to the PV emulator. In this scenario, the power supplied to the load solely depends on PV emulator settings.

Figure 4 shows the experimental setup connecting PV emulator, pc and lamp load. A panel whose specification matches with the PV emulator is taken to carry out experimentation. Accordingly, the simulation results of the kaneka panel are validated through experimentation.

Table 4. Specifications of the 62000H-S 600 programmable DC source

Parameters	Values
Range of voltage	0-600V
AC Power density module	5kW
Input voltage range	380/400Vac, 440/480Vac

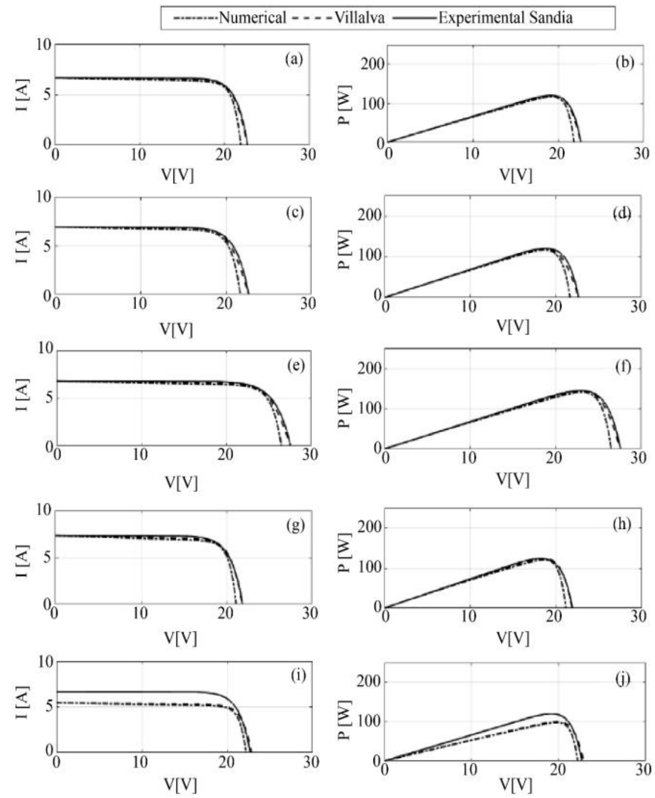

Fig. 3 I-V and P-V characteristics of 3 methods under STC, (a) & (b) Mono crystalline, (c) & (d) Polycrystalline, (e) & (f) PERC, (g) & (h) TOPCon, and (i) & (j) HJT.

Fig. 4 Hardware bench setup solar PV emulator with load

Figure 5 illustrates the simulation of I-V/P-V curves at various irradiances using the Kaneka panel's extracted values. Whereas in experimentation, the specifications are entered in a Sandia Excel sheet provided by Chroma, and uploading the sheet on a soft panel gives I-V/P-V curves. The testing is done with different irradiances.

Table 5. Experimental values from solar PV emulator

Irradiance(W/m^2)	V_{mp}	I_{mp}	V_{oc}	I_{sc}	P_{mp}	V_{mes}	I_{mes}	P_{mes}	MPPT (%η)
1000	53.37	1.896	71.01	2.250	101.2	67.14	0.744	50	49.34
800	52.26	1.531	67.06	1.723	80	63.362	0.722	45.7	57.15
600	50.01	1.2	64.18	1.351	60	59.434	0.6973	41.4	69.03
400	46.84	0.854	60.11	0.961	40	53.05	0.6567	34.8	87.06
300	44.59	0.673	57.22	0.757	30	47.225	0.6187	29.2	97.36
250	43.42	0.576	55.39	0.652	25	42.28	0.5848	24.7	98.78

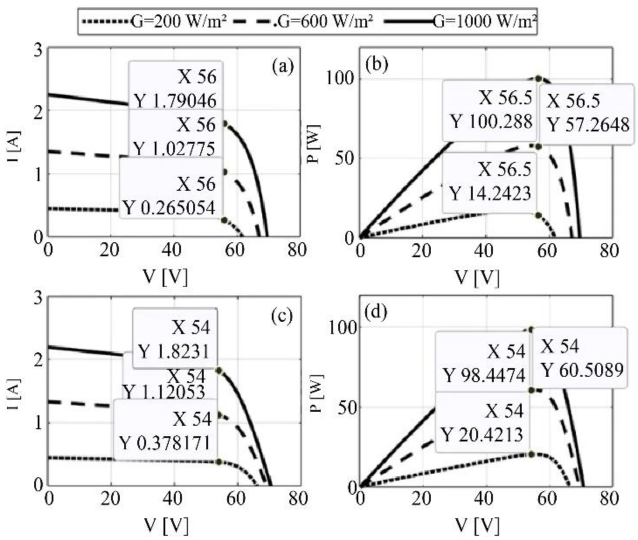

Fig. 5 I-V and P-V characteristics of kaneka under different irradiances, (a) & (b) Numerical method, and (c) & (d) Villalva method.

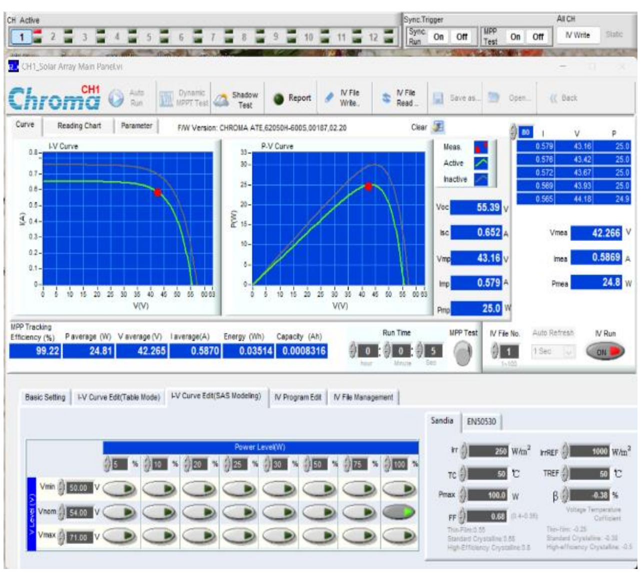

Fig. 6 I-V and P-V characteristics of kaneka with measured power point using solar PV emulator

The experimental I-V/P-V curves for irradiance change are shown in Figure 6. In Figure 6, it is to be noted that the grey curve corresponds to 300 W/m2, and the green curve corresponds to 250 W/m2. Figure 6 illustrates how the (red) point for load power shifts on the I-V/P-V curve when the irradiance drops from 300 W/m2 to 250 W/m2. When the load power and panel power are equal, the PowerPoint and peak positions coincide. This situation is exclusive to a certain power or irradiance level. Table 5 lists the measured load voltage, load current, and power delivered to the load. From Table 5, it is evident that the measured power matches panel power at 250 W/m2. When measured power is at its peak position, the efficiency of the MPPT test is high and close to 100%.

5.3. Models Accuracy and Performance Assessment

Figure 7 shows I-V and P-V curves at the 250 W/ m2 irradiance obtained in simulation and experiment. Figure 7 shows that the peak power of villalva is very close to the experimental value compared to the numerical approach. The Root Mean Square Error (RMSE) is calculated across a large number of operational locations to evaluate the accuracy of proposed methods. Six distinct test settings are examined in this section: G = 1000 W/m^2, 800 W/m^2, 600 W/m^2, 400 W/m^2, 300 W/m^2, and 250 W/m^2 at T = 25 °C.

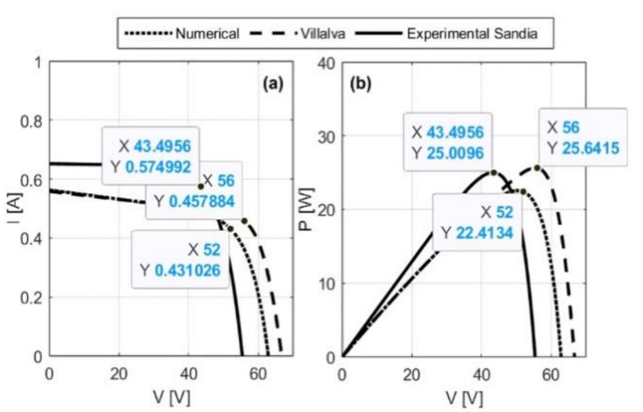

Fig. 7 (a) I-V, and (b) P-V characteristics of kaneka at G= 250 W/m^2.

Table 6. RMSE, MAE, MBE, and mean relative errors at different irradiance (W/m²)

Irradiance (W/m²)	Method	Error							
		RMSE (%)	MAE	MBE	EV_{mp} (V)	EI_{mp}(A)	EP_{mp}(W)	EV_{oc}(V)	EI_{sc}(A)
1000	A	0.2159	0.022896	-0.02278	0.011804	-0.01371	-0.00889	-0.00014	0
	B	0.82127	0.109444	-0.05583	0.011804	-0.01371	-0.0271	-0.01422	0
800	A	0.3674	0.044039	-0.044689	0.033295	0.52678	-0.01296	0.058664	0.044689
	B	0.3387	0.04987	-0.04987	0.033295	0.52678	-0.00128	-0.00089	0.023731
600	A	0.1439	0.015746	-0.0147	0.079784	1.59725	-0.03355	0.106061	-0.00074
	B	0.1266	0.018476	0.004135	0.079784	1.59725	0.012083	0.05952	-0.01674
400	A	0.3103	0.036832	0.018416	0.152861	4.4742390	-0.06288	0.180769	-0.06348
	B	0.3376	0.036249	0.035163	0.152861	4.474239	0.005975	0.147896	-0.07431
300	A	0.4113	0.055547	0.026465	0.21103	8.261961	-0.08383	0.240283	-0.10832
	B	0.4297	0.055145	0.033032	0.211034	8.261516	0.026167	0.21461	-0.11648
250	A	0.44607	0.056804	0.032705	0.243667	11.98611	-0.09728	0.28117	-0.13727
	B	0.4545	0.057231	0.036699	0.243667	11.98611	0.02652	0.263766	-0.14406
A- Numerical Method B- Villalva Method									

A common metric for evaluating a model's prediction accuracy is RMSE. It calculates the difference between the observed values and the values predicted by the model. RMSE provides an estimate of the errors' size. Larger mistakes significantly impact the RMSE number. It is simpler to compare RMSE across various models and datasets when it is expressed as a percentage with respect to the Highest Power Point Current (Imp). Lower RMSE values imply that the projected values align more with the actual values, indicating superior model performance. The RMSE values were obtained using the following formulas:

$$\mathrm{RMSE}(\%) = 100\frac{\sqrt{\frac{1}{N}\sum_1^N\left(I_{exp} - I_{model}\right)^2}}{I_{mp}} \tag{44}$$

Where I_{exp} is the experimental current value, I_{model} is the current value provided by the models, N is the number of experimental data points and I_{mp} is the current at the maximum power point. MAE determines the average magnitude of the absolute discrepancies between the modelled and tested current values without considering direction. It shows clearly how well the predicted values match the experimental values. The model's ability to properly depict the behaviour of PV panels at various operating points is shown by a reduced MAE. Using the following formula, the MAE is determined:

$$\mathrm{MAE}=\frac{1}{N}\sum_1^N\left|\left(I_{exp} - I_{model}\right)\right| \tag{45}$$

The average bias or systematic error between the modelled and experimental values is measured using MBE. In contrast to MAE, MBE takes into account the error's direction, revealing whether the model consistently overestimates or underestimates the true values. An underestimation is indicated by a negative MBE, whereas a positive MBE implies that the model tends to overestimate. The following formula is used to determine the MBE:

$$\mathrm{MBE}=\frac{1}{N}\sum_1^N\left(I_{exp} - I_{model}\right) \tag{46}$$

The Mean Relative Error (MRE) of estimated parameters is another crucial indicator for assessing how well various models work. MRE calculates how close the model's predictions are to the actual values that were observed. It offers a normalized measure of inaccuracy that facilitates comparisons across various scales. MRE can assist in locating persistent biases within the model. Overestimation is shown by positive values, and underestimating is indicated by negative numbers. MRE makes it simple to compare the performance of various models on the same dataset by reporting the error as a percentage. MRE is very helpful in determining if the model's predictions are proportionately correct and closely spaced in size. These measures are critical for evaluating the efficacy and dependability of models, particularly in domains where precise forecasts are necessary for efficient energy management and optimization, such as microgrids and solar PV systems. This is how the mean relative error is shown:

$$E_Y(\%) = 100\frac{Y_{model} - Y_{exp}}{Y_{exp}} \tag{47}$$

Where the extracted and experimental parameters are denoted by Y_{model} and Y_{exp}, for comparison, all parameters are set to Y = [V_{mp}, I_{mp}, P_{mp}, V_{oc}, I_{sc}]. Table 6 shows the RMSE and mean relative error of two different methods using the Kaneka datasheet at different irradiances. From Table 6, it is observed that as irradiance decreases, RMSE, MAE, MBE and E_Y (%) slightly increase. Though so, the RMSE and EY (%) are low, indicating that the simulation and experimental results closely match.

6. Conclusion

This paper presents a simple approach for obtaining a PV cell's SDM parameters. This study contributes to precisely estimating the amount of power generated under different operating conditions by creating a robust and adaptable PV model. This is essential for maximizing PV system performance and design. In order to extract parameters (I_{pv}, I_o, n, R_s and R_p), numerical and villalva approaches are utilized. Five unknown parameters are computed in general instances (any temperature and irradiance) based on the reference values of the unknown parameters determined at STC. For parameter extractions under conventional test settings, six distinct kinds of datasheets, namely monocrystalline, polycrystalline, PERC, Topcon, HJT, and kaneka, are employed. This study offers a more comprehensive and realistic assessment under various irradiance and temperature settings, in contrast to many state-of-the-art techniques evaluated on a small dataset or concentrating on a particular modelling methodology. Simulation and experimental results are compared to validate the derived parameters from these two approaches.

This comparison study aids in choosing the most effective technique for various PV cell types, enhancing system efficiency as a whole. Of these two approaches, villalva shows a very close match to experimental data compared to the numerical approach. The results of the simulations acquire credibility when they are validated by hardware experimental outputs, especially when the Chroma PV Emulator is utilized. The 62000H-S 600 solar PV emulator is used to retrieve the results of the experiments. This practical approach guarantees that the theoretical frameworks are based on actual performance in the real world. The testing is done with different irradiances. Achieving a 98.78% MPPT test efficiency and using the RMSE estimate to evaluate the mathematical techniques' precision shows how accurate and dependable the models were. This degree of accuracy is necessary to minimize financial and reliability risks while maximizing PV system performance.

7.1. Future Scope

This research presents new opportunities for further study, including investigating alternative PV technologies, refining parameter extraction techniques, combining PV systems with other renewable energy sources and enhancing PV system performance in diverse environments.

Data Availability Statement

The author(s) confirms that all data generated or analyzed during this study are included in this article. The data (six different types of manufacturing data sheets) that support the findings of this study are openly available at,

- Mono crystalline sesm12120(solex) solar data sheet available from: "https://www.enfsolar.com/pv/panel-datasheet/crystalline/51673", [42]
- Poly crystalline SES12120(SOLEX)solar data sheet available from:
- "https://cdn.energypal.com/panels/ses12120/energypal-solar-panel-spec-datasheet-solex-energy-25w-100w-36-cells-poly-ses12120.pdf.", [43].
- PERC sp-m10/40h solar panel datasheet available from: "https://www.enfsolar.com/pv/panel datasheet/crystalline/61037.", [44].
- TOPCON-ETFE solar panel series available from: "https://www.enfsolar.com/pv/panel-datasheet/crystalline/56692.", [45].
- HJT -FLEX-HDT solar panel available from: "https://www.enfsolar.com/pv/panel-datasheet/crystalline/55884.", [46].
- Kaneka solar panel available from: "https://www.kaneka-solar.com/product/thin-film/pdf/U-SA.pdf.", [47].

Author Contributions Statement

K.N. Yogithanjali Saimadhuri contributed to the mathematical modeling of the single diode model. M.Janaki & K.N.Yogithanjali Saimadhuri involved in determining five unknowns I_{pvref}, I_{oref}, n_{ref}, R_{sref}, and R_{pref} is done at general and reference conditions through two methods (Numerical and Villalva). K.N. Yogithanjali Saimadhuri compared six different solar PV panels (monocrystalline, polycrystalline, PERC, Topcon, HJT, and Kaneka). M. Janaki & K.N. Yogithanjali Saimadhuri investigated solar PV cells' I-V and P-V characteristics at various temperatures and irradiance levels and compared simulation results with hardware experimental outputs. The experiment uses the Chroma PV Emulator (62000H-S Series) to conduct a practical test. K.N. Yogithanjali Saimadhuri calculated root mean square error (RMSE) over a large number of operational locations to evaluate the accuracy of two mathematical techniques. K.N. Yogithanjali Saimadhuri wrote the manuscript under the supervision of M. Janaki.

References

[1] Alexandra Catalina Lazaroiu et al., "A Comprehensive Overview of Photovoltaic Technologies and their Efficiency for Climate Neutrality," *Sustainability*, vol. 15, no. 23, pp. 1-24, 2023. [CrossRef] [Google Scholar] [Publisher Link]

[2] Yi Wu, Jongwoo Lim, and Ming-Hsuan Yang, "Online Object Tracking: A Benchmark," *Proceedings of the IEEE Conference on Computer Vision and Pattern Recognition*, pp. 2411-2418, 2013. [Google Scholar] [Publisher Link]

[3] Abdul Rauf et al., "The Current Developments and Future Prospects of Solar Photovoltaic Industry in an Emerging Economy of India," *Environmental Science and Pollution Research*, vol. 30, no. 16, pp. 46270-46281, 2023. [CrossRef] [Google Scholar] [Publisher Link]

[4] Modupeola Dada, and Patricia Popoola, "Recent Advances in Solar Photovoltaic Materials and Systems for Energy Storage Applications: A Review," *Beni-Suef University Journal of Basic and Applied Science*, vol. 12, no. 1, pp. 1-15, 2023. [CrossRef] [Google Scholar] [Publisher Link]

[5] T. Yuvaraj et al., "Enhancing Indian Practical Distribution System Resilience through Microgrid Formation and Integration of Distributed Energy Resources Considering Battery Electric Vehicle," *IEEE Access*, vol. 11, pp. 133521-133539, 2023. [CrossRef] [Google Scholar] [Publisher Link]

[6] Abhishek Sharma et al., "An Effective Method for Parameter Estimation of a Solar Cell," *Electronics*, vol. 10, no. 3, pp. 1-21, 2021. [CrossRef] [Google Scholar] [Publisher Link]

[7] Puteri Sarah Mohamad Saad, Muhammad Yasin Bin Kasbudi, and Hashimah Hashim, "I-V and P-V Solar Cell Characteristics Simulation for a Single Diode Photovoltaic," *IEEE International Conference in Power Engineering Application*, Shah Alam, Malaysia, 2022. [CrossRef] [Google Scholar] [Publisher Link]

[8] Chuanzhong Xu et al., "A Noniterative Parameter-Extraction Method for Single-Diode Lumped Parameter Model of Solar Cells," *IEEE Trans Electron Devices*, vol. 68, no. 9, pp. 4529-4535, 2021. [CrossRef] [Google Scholar] [Publisher Link]

[9] Hussein Sharadga, Shima Hajimirza, and Elmer PT Cari, "A Fast and Accurate Single-Diode Model for Photovoltaic Design," *IEEE Journal of Emerging and Selected Topics in Power Electronics*, vol. 9, no. 3, pp. 3030-3043, 2021. [CrossRef] [Google Scholar] [Publisher Link]

[10] Samkeliso Shongwe, and Moin Hanif, "Comparative Analysis of Different Single-Diode PV Modeling Methods," *IEEE Journal of Photovoltaics*, vol. 5, no. 3, pp. 938-946, 2015. [CrossRef] [Google Scholar] [Publisher Link]

[11] Muhammad Saqib Ali, and Syed Muhammad Raza Kazmi, "An Accurate Analytical Approach for the Parameterization of the Single Diode Model of Photovoltaic Cell," *arXiv Preprint*, 2020. [CrossRef] [Google Scholar] [Publisher Link]

[12] Hussein Mohammed Ridha et al., "A Novel Theoretical and Practical Methodology for Extracting the Parameters of the Single and Double Diode Photovoltaic Models," *IEEE Access*, vol. 10, pp. 11110-11137, 2022. [CrossRef] [Google Scholar] [Publisher Link]

[13] Zuowen Liao et al., "An Improved Differential Evolution to Extract Photovoltaic Cell Parameters," *IEEE Access*, vol. 8, pp. 177838-177850, 2020. [CrossRef] [Google Scholar] [Publisher Link]

[14] Peng Hao, and Yunpeng Zhang, "An Improved Method for Parameter Identification and Performance Estimation of PV Modules from Manufacturer Datasheet Based on Temperature-Dependent Single-Diode Model," *IEEE Journal of Photovoltaics*, vol. 11, no. 6, pp. 1446-1457, 2021. [CrossRef] [Google Scholar] [Publisher Link]

[15] Weng-Hooi Tan, and Junita Mohamad-Saleh, "Critical Review on Interrelationship of Electro-Devices in PV Solar Systems with their Evolution and Future Prospects for MPPT Applications," *Energies*, vol. 16, no. 2, pp. 1-37, 2023. [CrossRef] [Google Scholar] [Publisher Link]

[16] Ashish K. Panchal, "I-V Data Operated High-Quality Photovoltaic Solution through Per-Unit Single-Diode Model," *IEEE Journal of Photovoltaics*, vol. 10, no. 4, pp. 1175-1184, 2020. [CrossRef] [Google Scholar] [Publisher Link]

[17] Efstratios Batzelis, "Non-Iterative Methods for the Extraction of the Single-Diode Model Parameters of Photovoltaic Modules: A Review and Comparative Assessment," *Energies*, vol. 12, no. 3, pp. 1-26, 2019. [CrossRef] [Google Scholar] [Publisher Link]

[18] Abdelkader Abbassi et al., "An Improved Single-Diode Model Parameters Extraction at Different Operating Conditions with a View to Modeling a Photovoltaic Generator: A Comparative Study," *Solar Energy*, vol. 155, pp. 478-489, 2017. [CrossRef] [Google Scholar] [Publisher Link]

[19] Mohamed Moutchou, and Younes Abouelmahjoub, "Model Parameters Identification of a Photovoltaic Module, Based on Fabricant Datasheet Information and By Using a Genetic Algorithm," *International Conference on Electrical, Computer, Communications and Mechatronics Engineering*, Mauritius, 2021. [CrossRef] [Google Scholar] [Publisher Link]

[20] T.R. Ayodele, A.S.O. Ogunjuyigbe, and E.E. Ekoh, "Evaluation of Numerical Algorithms Used in Extracting the Parameters of a Single-Diode Photovoltaic Model," *Sustainable Energy Technologies and Assessments*, vol. 13, pp. 51-59, 2016. [CrossRef] [Google Scholar] [Publisher Link]

[21] Henrique P. Corrêa, and Flávio H.T. Vieira, "Enhancing the Accuracy of an Explicit Solar Cell I-V Model via Low-Complexity Search-Based Parameter Extraction," *IEEE Access*, vol. 10, pp. 115823-115832, 2022. [CrossRef] [Google Scholar] [Publisher Link]

[22] F. Ghani et al., "The Numerical Calculation of Single-Diode Solar-Cell Modelling Parameters," *Renewable Energy*, vol. 72, pp. 105-112, 2014. [CrossRef] [Google Scholar] [Publisher Link]

[23] Lazuardi Umar et al., "Parasitic Resistance Calculation of PV Module at Various Irradiance Based on Three Condition Lambert-W," *4th International Seminar on Sensors, Instrumentation, Measurement and Metrology*, Padang, Indonesia, vol. 1528, 2020. [CrossRef] [Google Scholar] [Publisher Link]

[24] Yatindra Gopal et al., "Banes and Boons of Perturb & Observe, Incremental Conductance and Modified Regula Falsi Methods for Sustainable PV Energy Generation," *Journal of Power Technologies*, vol. 97, no. 1, pp. 35-43, 2017. [Google Scholar] [Publisher Link]

[25] Ali Kareem Abdulrazzaq, György Bognár, and Balázs Plesz, "Accurate Method for PV Solar Cells and Modules Parameters Extraction Using I-V Curves," *Journal of King Saud University-Engineering Sciences*, vol. 34, no. 1, pp. 46-56, 2022. [CrossRef] [Google Scholar] [Publisher Link]

[26] M.B.H. Rhouma, and A. Gastli, "An Extraction Method for the Parameters of the Solar Cell Single-Diode-Model," *2nd European Conference on Electrical Engineering and Computer Science*, Bern, Switzerland, pp. 433-437, 2018. [CrossRef] [Google Scholar] [Publisher Link]

[27] Abdelaaziz Benahmida, Noureddine Maouhoub, and Hassan Sahsah, “Numerical Approach for Extraction of Photovoltaic Generator Single-Diode Model Parameters,” *Computer Science and Information Technologies*, vol. 2, no. 2, pp. 58-66, 2021. [CrossRef] [Google Scholar] [Publisher Link]

[28] M.B. Prakash, and K.S. Reddy, “Understanding the Effect of Series Resistance for Solar PV Module,” *International Journal of Creative Research Thoughts*, vol. 6, no. 2, pp. 377-381, 2018. [Publisher Link]

[29] Marcelo Gradella Villalva, Jonas Rafael Gazoli, and Ernesto Ruppert Filho, “Comprehensive Approach to Modeling and Simulation of Photovoltaic Arrays,” *IEEE Transactions on Power Electronics*, vol. 24, no. 5, pp. 1198-1208, 2009. [CrossRef] [Google Scholar] [Publisher Link]

[30] B.K. Nayak, A. Mohapatra, and B. Misra, “Non-Linear I-V Curve of PV Module: Impacts on MPPT and Parameters Estimation,” *International Journal of Engineering Research & Technology*, vol. 1, no. 8, pp. 1-8, 2012. [Google Scholar] [Publisher Link]

[31] Tanvir Ahmad, Sharmin Sobhan, and Md Faysal Nayan, “Comparative Analysis between Single Diode and Double Diode Model of PV Cell: Concentrate Different Parameters Effect on Its Efficiency,” *Journal of Power and Energy Engineering*, vol. 4, no. 3, pp. 31-46, 2016. [CrossRef] [Google Scholar] [Publisher Link]

[32] Y. Chaibi et al., “Solar Irradiance and Temperature Influence on The Photovoltaic Cell Equivalent-Circuit Models,” *Solar Energy*, vol. 188, pp. 1102-1110, 2019. [CrossRef] [Google Scholar] [Publisher Link]

[33] Hitesh K. Mehta et al., “Accurate Expressions for Single-Diode-Model Solar Cell Parameterization,” *IEEE Journal of Photovoltaics*, vol. 9, no. 3, pp. 803-810, 2019. [CrossRef] [Google Scholar] [Publisher Link]

[34] J. Prasanth Ram et al., “Analysis on Solar PV Emulators: A Review,” *Renewable and Sustainable Energy Reviews*, vol. 81, pp. 149-160, 2018. [CrossRef] [Google Scholar] [Publisher Link]

[35] Driss Saadaoui et al., “Extraction of Single Diode PV Cell/Module Model Parameters Using a Hybrid BMO Approach with Lambert's W Function,” *International Journal of Ambient Energy*, vol.45, no. 1, 2024. [CrossRef] [Google Scholar] [Publisher Link]

[36] Ramzi Ben Messaoud, “Extraction of Uncertain Parameters of a Single-Diode Model for A Photovoltaic Panel Using Lightning Attachment Procedure Optimization,” *Journal of Computational Electronics*, vol. 19, pp. 1192-1202, 2020. [CrossRef] [Google Scholar] [Publisher Link]

[37] Jyoti Gupta, Parag Nijhawan, Souvik Ganguli, “Parameter Extraction of Solar PV Cell Models Using Novel Metaheuristic Chaotic Tunicate Swarm Algorithm,” *International Transactions on Electrical Energy Systems*, vol. 31, no. 12, 2021. [CrossRef] [Google Scholar] [Publisher Link]

[38] Amit Jain, and Avinashi Kapoor, “Exact Analytical Solutions of the Parameters of Real Solar Cells Using Lambert W-Function,” *Solar Energy Materials and Solar Cells*, vol. 81, no. 2, pp. 269-277, 2004. [CrossRef] [Google Scholar] [Publisher Link]

[39] M. Chegaar et al., “Determination of Solar Cells Parameters Under Illuminated Conditions,” *Journal of Electron Devices*, vol. 2, no. 1, pp. 17-21, 2003. [Google Scholar] [Publisher Link]

[40] Soteris A. Kalogirou, and Milorad Bojic, “Artificial Neural Networks for the Prediction of the Energy Consumption of a Passive Solar Building,” *Energy*, vol. 25, no. 5, pp. 479-491, 2000. [CrossRef] [Google Scholar] [Publisher Link]

[41] Raj Kumar Vinod, and S.K. Singh, “Solar Photovoltaic Modeling and Simulation: As a Renewable Energy Solution,” *Energy Reports*, vol. 4, pp. 701-712, 2018. [CrossRef] [Google Scholar] [Publisher Link]

[42] Ravi Prakash, and Sandeep Singh, “Designing and Modelling of Solar Photovoltaic Cell and Array,” *IOSR Journal of Electrical and Electronics Engineering*, vol. 11, no. 2, pp. 35-40, 2016. [Google Scholar] [Publisher Link]

[43] ENF Solar, 100-190W 36 Cells Mono, PV Panel Datasheet, 2024. [Online]. Available: https://www.enfsolar.com/pv/panel-datasheet/crystalline/51673

[44] ENF Solar, Solex Energy 25W-100W 36 Cells Poly SES12120 Solar Panel Spec Datasheet, 2024. [Online]. Available: https://www.enfsolar.com/pv/panel-datasheet/crystalline/42749

[45] ENF Solar, SP-M10/40H 145-150W, Solar Panel Datasheet-Crystalline, 2024. [Online]. Available: https://www.enfsolar.com/pv/panel-datasheet/crystalline/61037

[46] ENF Solar, SKT410~430M10-108D4, XXR-TOPCON-ETFE Solar Panel Series, 2024. [Online]. Available: https://www.enfsolar.com/pv/panel-datasheet/crystalline/56692

[47] ENF Solar, FLEX-HDT, SFED-F100HDT Solar Panel Datasheet, 2024. [Online]. Available: https://www.enfsolar.com/pv/panel-datasheet/crystalline/55884

[48] Kaneka Corporation, Building-Integrated Photovoltaics, Kaneka Solar Panel Datasheet-USA Series, 2024. [Online]. Available: https://www.kanekaenergysolutions.com/